Short communication

A constitutive model for spring-back prediction in which the change of Young's modulus with plastic deformation is considered

S.L. Zang[a,b,*], J. Liang[a], C. Guo[a]

[a]School of Mechanical Engineering, Xi'an Jiaotong University, No. 28, Xianning Road, Xi'an, Shaanxi, China
[b]State Key Laboratory of Plastic Forming Simulation and Die & Mould Technology, Wuhan 430074, China

Abstract

In order to improve the prediction capability of spring-back in the computational analysis of sheet metal forming processes, a stress–strain constitutive formulation of non-linear combined hardening rule has been proposed in this paper according to non-linear kinematic hardening theory of Lemaitre and Chaboche and Hill's 1948 anisotropic yielding function. Traditionally, Young's modulus is considered as a constant in engineering application and numerical simulation. In fact, it decreases with plastic deformation. So the effect of the change of Young's modulus with plastic strain on spring-back is considered in the constitutive model. The algorithm of stress update is elastic prediction, plastic correcting and radial returning. Numerical results and experimental results show that the proposed constitutive model significantly improves the prediction accuracy of spring-back.
© 2007 Elsevier Ltd. All rights reserved.

Keywords: Young's modulus; Spring-back; FEM; Constitutive model

1. Introduction

In recent years, the high strength steels and aluminum alloys, which have higher ratios of yield strength to elastic modulus, are increasingly used for sheet metal parts in automotive industry to reduce mass [1]. Hence, spring-back is one of the most important problem faced in sheet metal forming processes. Introducing computational methods based on the finite element method in the design stage is one way to reduce the try-error correct, especially utilizing proper mechanical properties of sheets [2].

Lems [3] revealed that Young's modulus decreases with plastic deformation. Due to the change of Young's modulus with plastic deformation, actual spring-back is larger than that computed with a constant Young's modulus. However, the most commercial FEM codes do not provide non-linear elastic and plastic constitutive model. To improve the spring-back prediction capability,

the relationship of plastic deformation and Young's modulus should be considered in numerical simulation. A variety of theoretical and experimental researches on the phenomenon of the change of Young's modulus with plastic deformation and elasto-plastic constitutive model have been investigated. Vin [4] gave a simple mathematical model describing the relationship between plastic deformation and Young's modulus based on experiment results. Morestin [5,6] formulated an elasto-plastic model using kinematic hardening model for spring-back analysis in sheet metal forming. In his calculations the change of the Young's modulus versus plastic strain was taken into account. Yan [7] addressed the effect of non-linear elastic unloading on spring-back prediction of V-shape bend.

Accurate spring-back prediction based on FEM also strongly depends on the hardening rule [1,8,9]. Isotropic hardening (IH) may not be so effective when the material points experience cyclic loads; for example, bending–unbending on the die shoulder and reverse bending–unbending at the punch [10]. The linear kinematic hardening proposed by Prager [11] and Ziegler [12] underestimates the spring-back because of the assumption of yield stress

---

*Corresponding author. School of Mechanical Engineering, Xi'an Jiaotong University, No. 28, Xianning Road, Xi'an, Shaanxi, China. Tel.: +86 29 82668607; fax: +86 29 82669103.
E-mail address: shunlai.zang@gmail.com (S.L. Zang).

surface without changing its shape and size. The Chaboche [13,14] model has gained some popularity because a recall term is introduced to realize the smooth elastic–plastic transition behavior in recent years. The combined isotropic-kinematic hardening law is considered suitable in predicting the spring-back [2,10].

The objective of the present study was to formulate an elasto-plastic constitutive equation based on the Chaboche non-linear kinematic (NLK) hardening rule and Hill's 1948 anisotropic yielding function. The Young's modulus has a significant influence on sheet spring-back. Usually, Young's modulus is considered as a constant in engineering application and numerical simulation, but it decreases with plastic deformation. So the change of Young's modulus with plastic strain is considered in the suggested constitutive model. A backward-Euler method with r-residual algorithm is utilized to update the stress increment. The constitutive equation for isotropic-kinematic hardening behaviors was implemented into the ABAQUS codes using the implicit user subroutine UMAT. The influences of hardening rules on the sheet spring-back are also discussed.

2. Constitutive model

The NLK hardening component of Chaboche combined hardening rule is adopted, with the exception that the steady-state evolution of α is given by Ziegler [12]:

$$\mathrm{d}\alpha_{ij} = \frac{C}{\sigma_e}(\sigma_{ij} - \alpha_{ij})\,\mathrm{d}\bar{\varepsilon}^p - \gamma\alpha_{ij}\,\mathrm{d}\bar{\varepsilon}^p, \tag{1}$$

where C and γ are NLK hardening material parameters. σ_{ij} is flow stress, and α_{ij} is back stress. σ_e, $\mathrm{d}\bar{\varepsilon}^p$, $\mathrm{d}\alpha_{ij}$ are the equivalent stress, equivalent plastic strain increment and back stress increment, respectively.

The single component form of IH rule is expressed by the following equation:

$$\sigma^0 = \sigma_0 + Q(1 - e^{-b\bar{\varepsilon}^p}), \tag{2}$$

where Q and b are IH material parameters, σ^0 is the current yield stress, σ_0 is the initial yielding stress and $\bar{\varepsilon}^p$ is the equivalent plastic strain.

The associated flow rule with Hill's 1948 anisotropic yield criterion is used in this investigation. The flow potential $f(\sigma_{ij}, \alpha_{ij})$ considering the Bauschinger effect can be written as

$$f = \sqrt{\tfrac{1}{2}(\sigma_{ij} - \alpha_{ij})K_{ijkl}(\sigma_{kl} - \alpha_{kl})} = \sigma_e \tag{3}$$

for plane stress problem the fourth-order tensor K_{ijkl} can be reformulated by a symmetric matrix P given in vector Voigt notation as

$$P = \begin{bmatrix} 1 & -\beta_{12} & 0 \\ -\beta_{12} & \beta_{22} & 0 \\ 0 & 0 & \beta_{66} \end{bmatrix}; \quad \sigma = \begin{bmatrix} \sigma_{11} \\ \sigma_{22} \\ \sigma_{12} \end{bmatrix}; \quad \alpha = \begin{bmatrix} \alpha_{11} \\ \alpha_{22} \\ \alpha_{12} \end{bmatrix}, \tag{4}$$

where the components of P can be related to the R-values as [10,15,16]

$$\beta_{12} = \frac{R_0}{1 + R_0},$$
$$\beta_{22} = \frac{R_0(1 + R_{90})}{R_{90}(1 + R_0)},$$
$$\beta_{66} = \frac{(R_0 + R_{90})(1 + 2R_{45})}{R_{90}(1 + R_0)}. \tag{5}$$

According to associated flow rule, plastic strain increment is

$$\mathrm{d}\varepsilon_{ij}^p = \mathrm{d}\lambda \frac{\partial f}{\partial \sigma_{ij}}, \tag{6}$$

where $\mathrm{d}\lambda$ is plastic multiplier.

The plastic work increment is shown in Eq. (7) as

$$\mathrm{d}w^p = (\sigma_{ij} - \alpha_{ij})\,\mathrm{d}\varepsilon_{ij}^p = \sigma_e\,\mathrm{d}\bar{\varepsilon}^p. \tag{7}$$

Using Euler's theorem for homogeneous function $f(\sigma_{ij}, \alpha_{ij})$, then

$$(\sigma_{ij} - \alpha_{ij})\frac{\partial f}{\partial \sigma_{ij}} = \sigma_e. \tag{8}$$

Substituting from Eq. (6) into Eq. (7), and combination with Eq. (8), the equivalent plastic strain increment can be written as

$$\mathrm{d}\bar{\varepsilon}^p = \mathrm{d}\lambda. \tag{9}$$

Decomposition of the strain increment $\mathrm{d}\varepsilon_{ij}$ into elastic component $\mathrm{d}\varepsilon_{ij}^e$ and plastic component $\mathrm{d}\varepsilon_{ij}^p$,

$$\mathrm{d}\varepsilon_{ij} = \mathrm{d}\varepsilon_{ij}^e + \mathrm{d}\varepsilon_{ij}^p. \tag{10}$$

Based on elastic Hooke's law,

$$\mathrm{d}\sigma_{ij} = C_{ijkl}^e\,\mathrm{d}\varepsilon_{kl}^e = C_{ijkl}^e(\mathrm{d}\varepsilon_{kl} - \mathrm{d}\varepsilon_{kl}^p), \tag{11}$$

where C_{ijkl}^e is elastic matrix, which can be written as

$$C_{ijkl}^e = \frac{E(\bar{\varepsilon}_A^p)}{1 + v}\left(\delta_{ik}\delta_{jl} + \frac{v}{1 - 2v}\delta_{ij}\delta_{kl}\right)$$
$$= 2G\delta_{ik}\delta_{jl} + \lambda\delta_{ij}\delta_{kl}, \tag{12}$$

where $E(\bar{\varepsilon}_A^p)$ and v are Young's modulus and Poisson ratio, G and λ are Lamé constants. δ_{ij} is Kronecker symbol. Since, the change of Young's modulus with plastic deformation is considered in the proposed constitutive model, the Young's modulus E in Eq. (12) is a function of equivalent plastic strain. $\bar{\varepsilon}_A^p$ is a known value during the incremental procedure.

The consistency condition can be stated as

$$\frac{\partial f}{\partial \sigma_{ij}}(\mathrm{d}\sigma_{ij} - \mathrm{d}\alpha_{ij}) = H\mathrm{d}\bar{\varepsilon}^p, \tag{13}$$

where H is $\mathrm{d}\sigma^0/\mathrm{d}\bar{\varepsilon}^p$.

Substituting from Eqs. (1), (6), (9) and (11) into Eq. (13):

$$\mathrm{d}\lambda = \frac{(\partial f/\partial \sigma_{ij})C_{ijkl}^e\,\mathrm{d}\varepsilon_{kl}}{(\partial f/\partial \sigma_{ij})C_{ijkl}^e(\partial f/\partial \sigma_{kl}) + C - \gamma(\partial f/\partial \sigma_{ij})\alpha_{ij} + H}. \tag{14}$$

The standard tangent modular can be obtained by substitution of Eq. (14) back into Eq. (11):

$$d\sigma_{ij} = C_{ijkl}^{ep} d\varepsilon_{kl}, \tag{15}$$

where C_{ijkl}^{ep} is standard tangent modular, which can be written as

$$C_{ijkl}^{ep} = C_{ijkl}^{e}$$
$$- \frac{C_{ijkl}^{e}(\partial f/\partial\sigma_{kl})C_{rskl}^{e}(\partial f/\partial\sigma_{rs})}{(\partial f/\partial\sigma_{ij})C_{ijkl}^{e}(\partial f/\partial\sigma_{kl}) + C - \gamma(\partial f/\partial\sigma_{ij})\alpha_{ij} + H}. \tag{16}$$

3. Numerical implementation

The numerical scheme to solve non-linear boundary value problems of sheet metal forming processes using FEM is to iteratively try out the discrete displacement increments at the discretized material space and process time until the trial values ultimately satisfy the equilibrium condition. Usually, the scheme consists of three steps. Firstly, the discrete strain increments are calculated from trial displacement increments and secondly, according to all constitutive variables at step (n) and $\Delta\varepsilon_{n+1}$, to solve σ_{n+1}, α_{n+1} and other variables at current step $n + 1$ using elasto-plastic constitutive equation. Finally, the tolerance is checked whether the equilibrium condition is satisfied. In the second step, the stresses update algorithm of elastic predicting, plastic correcting and radical returning is applied to adjust the stress and strain to satisfy the constitutive relation and yielding condition. The detailed update scheme is described as follows:

(1) The updated stress is initially assumed to be elastic for a given (n)th step discrete strain increment $\Delta\varepsilon_{n+1}$. Therefore,

$$\sigma_{n+1}^{T} = \sigma_n + C^e(\bar{\varepsilon}_n^p)\Delta\varepsilon_{n+1}, \tag{17}$$

where the superscript 'T' stands for a trial state and the subscript denotes the process time step. In certain time step, Young's modulus is fixed, which value is determined by $\bar{\varepsilon}_n^p$, so the elastic matrix is $C^e(\bar{\varepsilon}_n^p)$. Also, preserving the plastic quantities as the previous values,

$$\bar{\varepsilon}_{n+1}^{p(T)} = \bar{\varepsilon}_n^p, \quad \alpha_{n+1}^T = \alpha_n. \tag{18}$$

If the following yield condition is satisfied with the trial values for a prescribed elastic tolerance Tol^e,

$$f(\sigma_{n+1}^T, \alpha_{n+1}^T) - \sigma^0(\bar{\varepsilon}_{n+1}^{p(T)}) < \text{Tol}^e \tag{19}$$

the process at the step $n + 1$ is considered elastic.

(2) If the above condition on yielding is violated, the step is considered as elasto-plastic and the trial elastic stress is taken as an initial value for the solution of the plastic corrector problem. The plastic strain increments are obtained such that the following new trial stress stays on the new yield surface:

$$\sigma = \sigma_n + C^e(\bar{\varepsilon}_n^p)(\Delta\varepsilon_{n+1} - \Delta\varepsilon^p). \tag{20}$$

The new back stress can be written as

$$\alpha = \alpha_n + C\frac{\Delta\bar{\varepsilon}^p}{\sigma_e}(\sigma - \alpha) - \gamma\alpha\Delta\bar{\varepsilon}^p. \tag{21}$$

The $(n + 1)$th step Cauchy stress, back stress and other constitutive variables should make the following yielding condition hold:

$$f(\sigma, \alpha) - \sigma^0 = 0. \tag{22}$$

Eqs. (20)–(22) are non-linear equations, and generally it could not obtain the solutions directly. Here, Newton–Raphson's iterative method is used to solve $\Delta\lambda$. In order to derive such an iterative loop, r residuals are defined to represent the differences between the current constitutive variables and the backward-Euler ones, i.e.

$$r_\sigma = \sigma - \sigma_n - C^e(\bar{\varepsilon}_n^p)(\Delta\varepsilon_{n+1} - \Delta\varepsilon^p), \tag{23}$$

$$r_\alpha = \alpha - \alpha_n - \frac{C\Delta\bar{\varepsilon}^p}{\sigma_e}(\sigma - \alpha) + \gamma\alpha\Delta\bar{\varepsilon}^p, \tag{24}$$

$$r_f = f(\sigma, \alpha) - \sigma^0. \tag{25}$$

Eqs. (23)–(25) together with the plastic potential Eqs. (1), (6) and (9) define the complete set of equations which must be satisfied implicitly. Fixing $\Delta\varepsilon_{n+1}$, a truncated Taylor expansion can be applied to the above equations,

$$r_\sigma^t = r_\sigma + \dot{\sigma} + \dot{\lambda}C^e a + \Delta\lambda C^e\frac{\partial a}{\partial\sigma}\dot{\sigma} - \Delta\lambda C^e\frac{\partial a}{\partial\sigma}\dot{\alpha}, \tag{26}$$

$$r_\alpha^t = r_\alpha + \dot{\alpha} - \frac{C\Delta\dot{\bar{\varepsilon}}^p}{\sigma_e}\bar{\sigma} - \frac{C\Delta\bar{\varepsilon}^p}{\sigma_e}(\dot{\sigma} - \dot{\alpha}) + \frac{C\Delta\bar{\varepsilon}^p\dot{\sigma}_e}{\sigma_e^2}\bar{\sigma}$$
$$+ \Delta\dot{\bar{\varepsilon}}^p\gamma\alpha + \Delta\bar{\varepsilon}^p\gamma\dot{\alpha}, \tag{27}$$

$$r_f^t = r_f + \dot{\sigma}_e - A_i\Delta\dot{\bar{\varepsilon}}^p = r_f + a^T\dot{\sigma} - a^T\dot{\alpha} - A_i\Delta\dot{\bar{\varepsilon}}^p, \tag{28}$$

where the superscript 't' is used to denote the Taylor expansion, $\dot{\sigma}$ is the iterative change in σ, $\dot{\alpha}$ is the iterative change in α, $\Delta\dot{\bar{\varepsilon}}^p$ is the iterative change in $\Delta\bar{\varepsilon}^p$ and $\dot{\lambda}$ is the iterative change in $\Delta\lambda$, a is $\partial f/\partial\sigma$, $\bar{\sigma}$ is equal to $\sigma - \alpha$, A_i is equal to H.

From Eq. (9), we must have

$$\Delta\bar{\varepsilon}^p = \Delta\lambda, \tag{29}$$

$$\Delta\dot{\bar{\varepsilon}}^p = \dot{\lambda}. \tag{30}$$

By setting the left-hand sides of Eqs. (26)–(28) to zero, we can provide the basis for a Newton–Raphson iteration. In particular, substituting into Eq. (27) from Eq. (28) for $\dot{\sigma}_e$,

$$\dot{\alpha} = -D_1 r_\alpha + D_2\bar{\sigma} + D_3\bar{\sigma}\dot{\lambda} - D_1\gamma\alpha\dot{\lambda} + (1 - D_4)\dot{\sigma}, \tag{31}$$

where

$$\Delta\lambda' = \frac{\Delta\lambda}{\sigma_e}; \quad d = C\Delta\lambda'; \quad D_1 = \frac{1}{1 + d + \Delta\lambda\gamma},$$

$$D_2 = \frac{r_f d}{(1 + d + \Delta\lambda\gamma)\sigma_e}; \quad D_3 = \frac{C(1 - \Delta\lambda' A_i)}{(1 + d + \Delta\lambda\gamma)\sigma_e},$$

$$D_4 = \frac{1 + \Delta\lambda\gamma}{1 + d + \Delta\lambda\gamma}. \tag{32}$$

Substitution from Eq. (31) into Eq. (26) then leads to

$$\dot{\boldsymbol{\sigma}} = -\boldsymbol{\Theta}^{-1}\bar{\boldsymbol{r}} - \boldsymbol{\Theta}^{-1}\boldsymbol{C}^e\boldsymbol{a}\dot{\lambda} + \boldsymbol{\Theta}^{-1}\boldsymbol{\Gamma}\dot{\lambda}, \tag{33}$$

where

$$\boldsymbol{\Theta} = \boldsymbol{I} + D_4\Delta\lambda\boldsymbol{C}^e\frac{\partial\boldsymbol{a}}{\partial\boldsymbol{\sigma}}, \tag{34}$$

$$\bar{\boldsymbol{r}} = \boldsymbol{r}_\sigma + D_1\Delta\lambda\boldsymbol{C}^e\frac{\partial\boldsymbol{a}}{\partial\boldsymbol{\sigma}}\boldsymbol{r}_\alpha - D_2\Delta\lambda\boldsymbol{C}^e\frac{\partial\boldsymbol{a}}{\partial\boldsymbol{\sigma}}\bar{\boldsymbol{\sigma}}, \tag{35}$$

$$\boldsymbol{\Gamma} = D_3\Delta\lambda\boldsymbol{C}^e\frac{\partial\boldsymbol{a}}{\partial\boldsymbol{\sigma}}\bar{\boldsymbol{\sigma}} - D_1\Delta\lambda\gamma\boldsymbol{C}^e\frac{\partial\boldsymbol{a}}{\partial\boldsymbol{\sigma}}\boldsymbol{\alpha}. \tag{36}$$

In Eq. (34) $\boldsymbol{I}$ is fourth-order identity matrix.

Substituting from Eqs. (31) and (33) into Eq. (28), $\dot{\lambda}$ can be expressed as

$$\dot{\lambda} = \frac{r_f - \tilde{q}}{D_4\boldsymbol{a}^T\boldsymbol{\Theta}^{-1}\boldsymbol{C}^e\boldsymbol{a} + A_k + A_i}, \tag{37}$$

where

$$\tilde{q} = D_4\boldsymbol{a}^T\boldsymbol{\Theta}^{-1}\bar{\boldsymbol{r}} + D_2\sigma_e - D_1\boldsymbol{a}^T\boldsymbol{r}_\alpha, \tag{38}$$

$$A_k = D_3\sigma_e - D_1\gamma\boldsymbol{a}^T\boldsymbol{\alpha} - D_4\boldsymbol{a}^T\boldsymbol{\Theta}^{-1}\boldsymbol{\Gamma}. \tag{39}$$

Once the increment of consistent parameter $\dot{\lambda}$ is set with Eq. (37), then the $\dot{\boldsymbol{\sigma}}$, $\dot{\boldsymbol{\alpha}}$ are determined by Eqs. (31) and (33). The increments of constitutive state variables are

$$\boldsymbol{\sigma} = \boldsymbol{\sigma} + \dot{\boldsymbol{\sigma}}, \tag{40}$$

$$\boldsymbol{\alpha} = \boldsymbol{\alpha} + \dot{\boldsymbol{\alpha}}, \tag{41}$$

$$\Delta\lambda = \Delta\lambda + \dot{\lambda}, \tag{42}$$

$$\Delta\bar{\varepsilon}^p = \Delta\lambda. \tag{43}$$

Check yield criterion with updated constitutive values,

$$\Phi = f(\boldsymbol{\sigma}, \boldsymbol{\alpha}) - \sigma^0 \tag{44}$$

if it returns greater than tolerance Tol^e, repeat the iteration. If it returns less than or equal to the tolerance, then transfer the last iterative values to next step values and quit the iteration loop.

(3) Update the constitutive variables and calculate the tangent modulus matrix

$$\boldsymbol{\sigma}_{n+1} = \boldsymbol{\sigma}, \tag{45}$$

$$\boldsymbol{\alpha}_{n+1} = \boldsymbol{\alpha}. \tag{46}$$

$\Delta\bar{\varepsilon}^p_{n+1}$ can be determined by Eq. (9), thus

$$\bar{\varepsilon}^p_{n+1} = \bar{\varepsilon}^p_n + \Delta\bar{\varepsilon}^p_{n+1} = \bar{\varepsilon}^p_n + \Delta\lambda. \tag{47}$$

The consistent tangent modular matrix significantly improves the convergence characteristics of the overall equilibrium iterations if a Newton–Raphson scheme is used. Standard techniques would use the modular of Eq. (16) which is 'inconsistent' with the backward-Euler integrations scheme and hence destroys the 'quadratic convergence' inherent in the Newton–Raphson method [17,18]. Here, the consistent tangent modular is derived by the consistent linearization of the update scheme.

The equilibrium state 'b' is known, the new state 'c' at the end of increment will be calculated. The tangent modular can be defined as

$$\boldsymbol{C}^{ep} = \frac{\partial\dot{\boldsymbol{\sigma}}}{\partial\dot{\boldsymbol{\varepsilon}}}\bigg|_c, \tag{48}$$

where '·' stand for time derivative.

Considering Eqs. (20) and (21), the standard backward-Euler algorithm can be written as

$$\boldsymbol{\sigma} = \boldsymbol{\sigma}^T - \Delta\lambda\boldsymbol{C}^e\boldsymbol{a}, \tag{49}$$

$$\boldsymbol{\alpha} = \boldsymbol{\alpha}_b + \frac{C\Delta\lambda}{\sigma_e}(\boldsymbol{\sigma} - \boldsymbol{\alpha}) - \gamma\boldsymbol{\alpha}\Delta\lambda, \tag{50}$$

$$\phi = f(\boldsymbol{\sigma}, \boldsymbol{\alpha}) - \sigma^0 = 0 \tag{51}$$

for the convenient, we dropped the suffix 'c' relating to the current configuration.

Differentiation of Eqs. (49)–(51) gives

$$\dot{\boldsymbol{\sigma}} = \boldsymbol{C}^e\dot{\boldsymbol{\varepsilon}} - \dot{\lambda}\boldsymbol{C}^e\boldsymbol{a} - \Delta\lambda\boldsymbol{C}^e\frac{\partial\boldsymbol{a}}{\partial\boldsymbol{\sigma}}\dot{\boldsymbol{\sigma}} + \Delta\lambda\boldsymbol{C}^e\frac{\partial\boldsymbol{a}}{\partial\boldsymbol{\sigma}}\dot{\boldsymbol{\alpha}}, \tag{52}$$

$$\dot{\boldsymbol{\alpha}} = \frac{C\dot{\lambda}}{\sigma_e}\bar{\boldsymbol{\sigma}} + \frac{C\Delta\lambda}{\sigma_e}(\dot{\boldsymbol{\sigma}} - \dot{\boldsymbol{\alpha}}) - \frac{C\Delta\lambda}{\sigma_e^2}\dot{\sigma}_e\bar{\boldsymbol{\sigma}} - \dot{\lambda}\gamma\boldsymbol{\alpha} - \Delta\lambda\gamma\dot{\boldsymbol{\alpha}}, \tag{53}$$

$$\dot{\phi} = \dot{\sigma}_e - A_i\dot{\lambda} = \boldsymbol{a}^T(\dot{\boldsymbol{\sigma}} - \dot{\boldsymbol{\alpha}}) - A_i\dot{\lambda} = 0. \tag{54}$$

Substituting into Eq. (53) from Eq. (54) for $\dot{\sigma}_e$,

$$\dot{\boldsymbol{\alpha}} = D_3\bar{\boldsymbol{\sigma}}\dot{\lambda} + (1 - D_4)\dot{\boldsymbol{\sigma}} - D_1\gamma\dot{\lambda}\boldsymbol{\alpha}. \tag{55}$$

Substituting from Eq. (55) into Eq. (52),

$$\dot{\boldsymbol{\sigma}} = \boldsymbol{R}\dot{\boldsymbol{\varepsilon}} - \boldsymbol{R}\boldsymbol{a}\dot{\lambda} \textcolor{red}{+} \boldsymbol{\Theta}^{-1}\boldsymbol{\Gamma}\dot{\lambda}, \tag{56}$$

where $\boldsymbol{R}$ is $\boldsymbol{\Theta}^{-1}\boldsymbol{C}^e$.

Substitution from Eqs. (55) and (56) into Eq. (54), thus

$$\dot{\lambda} = \frac{D_4\boldsymbol{a}^T\boldsymbol{\Theta}^{-1}\boldsymbol{C}^e\dot{\boldsymbol{\varepsilon}}}{D_4\boldsymbol{a}^T\boldsymbol{\Theta}^{-1}\boldsymbol{C}^e\boldsymbol{a} + A_k + A_i}$$

$$= \frac{\boldsymbol{a}^T\boldsymbol{\Theta}^{-1}\boldsymbol{C}^e\dot{\boldsymbol{\varepsilon}}}{\boldsymbol{a}^T\boldsymbol{\Theta}^{-1}\boldsymbol{C}^e\boldsymbol{a} + A_k' + A_i'}. \tag{57}$$

In the first relationship in Eq. (57) D_4 are from Eq. (32). The final relationship, which is obtained after some algebraic manipulation is of an identical form.

Substitution from Eq. (57) into Eq. (56) then leads to the consistent tangential relationship whereby

$$\boldsymbol{C}^{ep} = \boldsymbol{R} - \frac{\boldsymbol{\Lambda}\boldsymbol{a}^T\boldsymbol{R}}{\boldsymbol{a}^T\boldsymbol{R}\boldsymbol{a} + A_k' + A_i'}, \tag{58}$$

where

$$\Lambda = Ra - \Theta^{-1}\Gamma. \tag{59}$$

4. Results and discussion

The draw-bead simulator provides important information about the deformation of metal sheet under multiple bending and stretching processes. The 3-D plane stress draw-bead problem as shown in Fig. 1 is a case studied in the current paper. And the spring-back parameters of h and θ studied by this research are shown in Fig. 2. The sheet blank dimension is 250 mm in length, 50 mm in width, and 1.3 mm in thickness. After clamping the blank between the upper and lower die, the sheet is pulled 50 mm to the right

Fig. 1. Die shape and dimensions for the draw-bead test.
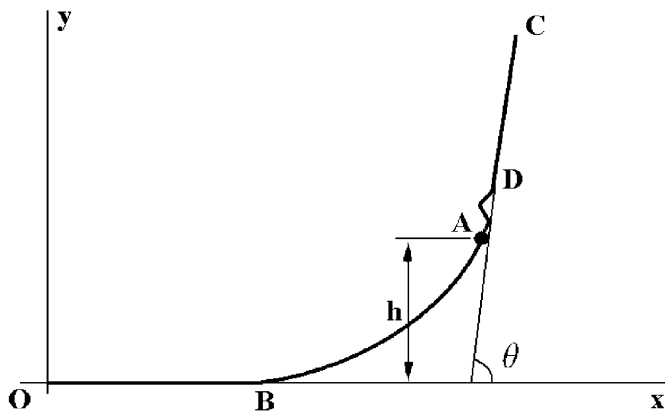
Fig. 2. Spring-back definition for the draw-bead test.

at a constant drawing speed of 5 mm/s. The clamping force is 6.8 kN, and the friction coefficient between the sheet and tools is 0.15. The material is AA2024-T3 aluminum alloy and the material parameters are summarized in Table 1. Since the change of Young's modulus with plastic deformation is considered, the Young's modulus is approximated by a piecewise linear function of equivalent plastic strain, which can be described as

$$E(\bar{\varepsilon}^{p}) = \begin{cases} E_{\text{init}} - \dfrac{(E_{\text{init}} - E_{\text{stab}})\bar{\varepsilon}^{p}}{\bar{\varepsilon}_{*}^{p}}, & 0 \leqslant \bar{\varepsilon}^{p} \leqslant \bar{\varepsilon}_{*}^{p}, \\ E_{\text{stab}}, & \bar{\varepsilon}_{*}^{p} \leqslant \bar{\varepsilon}^{p}, \end{cases} \tag{60}$$

where E_{init}, E_{stab} and $\bar{\varepsilon}_{*}^{p}$ are material parameters, respectively. The details on piecewise linear function and experiment method can be found in Ref. [5] and authors' work [19].

The material models were implemented via the UMAT interface of ABAQUS utilizing a backward-Euler algorithm for integration of the incremental plasticity equations and a consistent tangent matrix derived from this algorithm for Newton–Raphson iteration. Quadrilateral shell element (S4R, a uniform mesh of 150 elements in the length direction and 5 in the width direction) are used with 15 Simpson integration points through the thickness. Three hardening rules, which are IH model, NLK hardening model and isotropic/non-linear kinematic (INLK) hardening model of Chaboche type, are utilized in the paper.
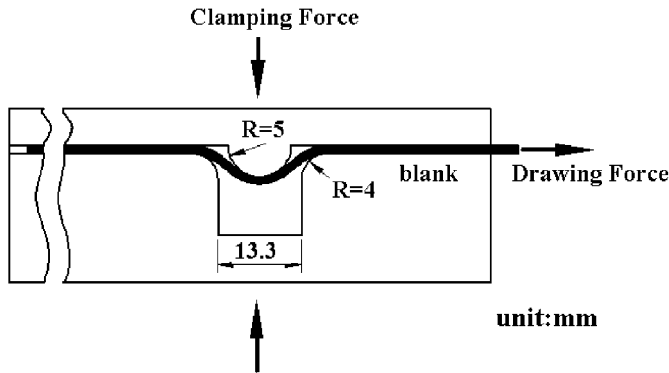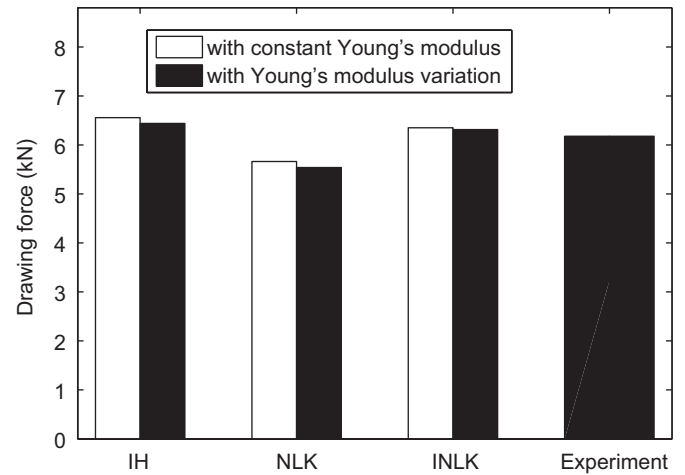

Fig. 3. Comparison of simulation drawing force of different hardening rules with measured data.

Table 1
Material parameters of AA2024-T3

Material models	C (MPa)	γ	r_0	r_{45}	r_{90}	σ_0 (MPa)	Q (MPa)	b	E_{init} (GPa)	E_{stab} (GPa)	$\bar{\varepsilon}_{*}^{p}$	v
IH	N/A	N/A	0.790	1.014	0.797	325.7	232.5	9.05	70	56	0.04	0.33
NLK	2104.13	9.05	0.790	1.014	0.797	325.7	N/A	N/A	70	56	0.04	0.33
INLH	924.8	8.9	0.790	1.014	0.797	325.7	128.9	9.2	70	56	0.04	0.33
Tensile test	N/A	N/A	0.790	1.014	0.797	325.7	N/A	N/A	70	56	0.04	0.33

The effect of different hardening rules on the drawing force is shown in Fig. 3. The predicted drawing force from the IH model is higher than the experimental data because the Bauschinger effect at reversal loading is ignored. The NLK model predicted lower drawing force since the overestimated Bauschinger effect is modeled. The simulated results considered the change of Young's modulus with plastic deformation are slightly lower than those with constant Young's modulus. The simulation results obtained with INLK model agree well with experiments for drawing force.
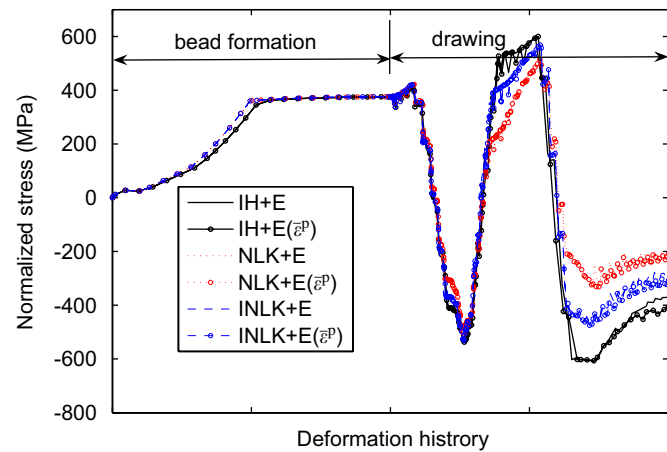
Fig. 4. The effect of different hardening rules on the tangential stress of integral points near top surface.
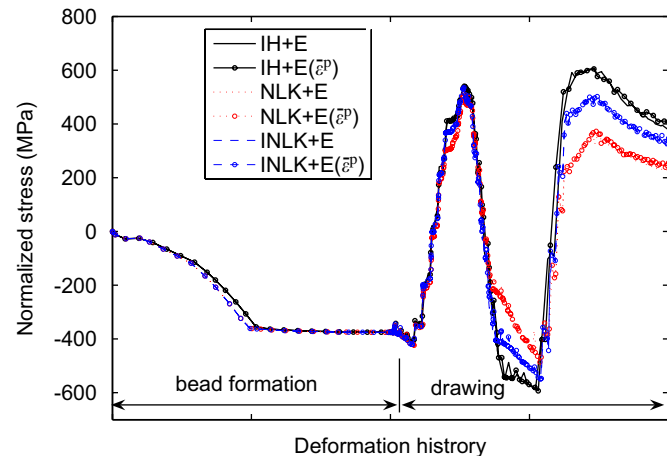
Fig. 5. The effect of different hardening rules on the tangential stress of integral points near bottom surface.

Because spring-back is proportional to moment and inverse to modulus, an accurate stress distribution is essential in the prediction of the amount of spring-back. The tangential stresses of Simpson integral points near the top surface and bottom surface are traced during the deformation in Figs. 4 and 5, respectively. A cyclic bending and unbending are observed during the drawing stage for all models. However, the INLK model predict a suitable drop in the stress when the monitored material point pass the draw-bead region due to the Bauschinger effect is correctly modeled. A conclusion can be drawn from Figs. 4 and 5 that the tangential stress for INLK hardening rule is less than that for IH model, but larger than that for NLK model. Although the differences of simulation results with a constant Young's modulus and with a variable Young's modulus are not distinct for all three hardening models, we cannot extend this to a more complicated forming process. The stress distribution is based on suitable constitutive model in the numerical simulation.

For the Hill's 1948 anisotropy yield function and shell element S4R, the influences of different hardening rules on sheet spring-back are shown in Table 2. And Fig. 6 presents the simulation results for corresponding location of nodes on the middle surface after sheet spring-back. Fig. 7 shows experiment spring-back of the blank when the punch is removed and inserts of draw-bead test device. It can be seen from Table 2 and Fig. 6 that the numerical simulation spring-back with variable Young's modulus is larger than that with constant Young's modulus for all three hardening models. Since the stresses distribution obtained from the same hardening model are similar as mentioned above, then the spring-back is mainly inverse to Young's modulus. The sheet spring-back is the least for NLK hardening model, then for INLK hardening model, and is the largest for IH model. The simulation results, especially the sheet spring-back obtained with the INLK hardening, in which the change of Young's modulus with plastic deformation is considered, agree well with experiments.

5. Conclusion

In this paper, an elasto-plastic constitutive model based on INLK rule and Hill's 1948 anisotropic yield function, where the change of Young's modulus with plastic strain is considered, is proposed. The backward-Euler method with R-residual algorithm is used in this study to integrate the rate form of constitutive equation. The effect of different

Table 2
The effect of hardening rules on sheet spring-back

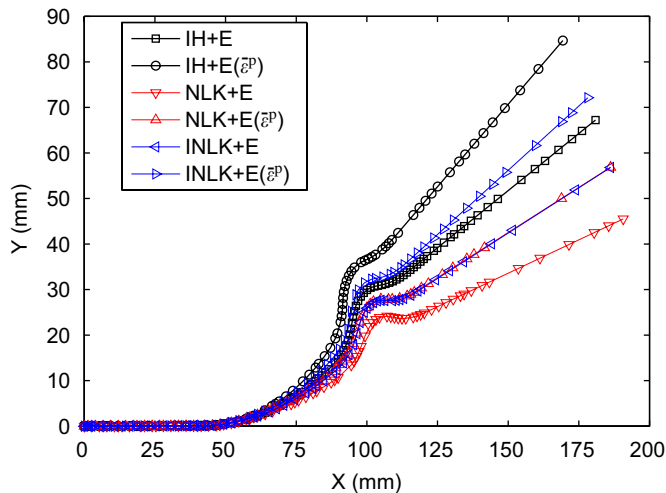|	IH E	IH $E(\bar{\varepsilon}^{p})$	NLK E	NLK $E(\bar{\varepsilon}^{p})$	INLK E	INLK $E(\bar{\varepsilon}^{p})$	Experiment data
h (mm)	15.56	19.26	11.90	14.28	13.91	16.91	15.0–18.6
θ (deg)	26.62	35.87	16.14	21.48	21.41	29.39	27.0–33.5

Fig. 6. The sheet spring-back of middle surface under different material hardening rules.

Fig. 7. Experiment results and inserts of draw-bead test device.

hardening models on sheet spring-back has been discussed. The study indicates that the IH law overestimate the Bauschinger effect, when the NLK is used, the spring-back amount is considerably underestimated, suggesting that kinematic hardening is not adequate to predict the spring-back. Numerical results and experimental results show that an accurate modeling of Bauschinger effect and the change of Young's modulus with plastic deformation appear to be more important when multiple cycles of bending–reverse bending loading conditions are expected.

Although the current constitutive model with a variable Young's modulus was only verified for draw-bead forming, its application to more complex parts is expected also to yield accurate results.

References

[1] D.J. Zhang, Z.S. Cui, X.Y. Ruan, Y.Q. Li, Sheet spring-back prediction based on non-linear combined hardening rule and Barlat89's yielding function, Computational Materials Science 38 (2006) 256–262.

[2] K. Chung, M.G. Lee, D. Kim, et al., Spring-back evaluation of automotive sheets based on isotropic-kinematic hardening laws and non-quadratic anisotropic yield functions, Part I: Theory and formulation, International Journal of Plasticity 21 (2005) 861–882.

[3] W. Lems, The change of Young's modulus after deformation at low temperature and its recovery, Ph.D. Dissertation, Delft, 1963.

[4] L.J. Vin, A.H. Streppl, U.P. Singh, A process model for air bending, Journal of Materials Processing Technology 56 (1996) 48–54.

[5] F. Morestin, M. Boivin, C. Silva, Elasto-plastic formulation using a kinematic hardening model for spring-back analysis in sheet metal forming, Journal of Materials Processing Technology 56 (1996) 619–630.

[6] F. Morestin, M. Boivin, On the necessity of taking into account the variation in Young's modulus with plastic strain in elastic–plastic software, Nuclear Engineering and Design 162 (1996) 107–116.

[7] L.C. Yan, B.Y. Xu, The effect of non-linear elastic unloading on spring-back prediction, Mechanics in Engineering 24 (2002) 41–43.

[8] J.T. Gau, G.L. Kinzel, A new model for spring-back prediction in which the Bauschinger effect is considered, International Journal of Mechanical Sciences 43 (2001) 1813.

[9] K.P. Li, W.P. Carden, R.H. Wagoner, Simulation of spring-back, International Journal of Mechanical Sciences 44 (2002) 103.

[10] B.K. Chun, Study on hardening models and numerical implementation for spring-back prediction, Ph.D. Dissertation, The Ohio State University, 2001.

[11] W. Prager, A new method of analyzing stresses and strains in work hardening solids, ASME Journal of Applied Mechanics 78 (1956) 493.

[12] H. Ziegler, A modification of Pragers hardening rule, Quarterly of Applied Mathematics 17 (1959) 55–65.

[13] J. Lemaitre, J.L. Chaboche, Mechanics of Solid Materials, Cambridge University Press, Cambridge, 1990.

[14] J.L. Chaboche, Constitutive equations for cyclic plasticity and cyclic visco-plasticity, International Journal of Plasticity 5 (1989) 247.

[15] S. Valliappan, P. Boonlaulohr, I.K. Lee, Non-linear analysis for anisotropic material, International Journal for Numerical Methods in Engineering 10 (1976) 597–606.

[16] K.P. Li, Contribution to the finite element simulation of three-dimensional sheet metal forming, Ph.D. Dissertation, University de Liege, 1996.

[17] M.A. Crisfield, Non-linear Finite Element Analysis of Solids and Structures, vol. 1, Wiley, New York, 1991.

[18] M.A. Crisfield, Non-linear Finite Element Analysis of Solids and Structures, vol. 2, Wiley, New York, 1997.

[19] S.L. Zang, C. Guo, G.J. Wei, et al., A new model to describe the effect of plastic deformation on Young's modulus of aluminum alloy, Transactions of Nonferrous Metals Society of China (2006) SP3.